https://doi.org/10.1117/12.2307831

Photonic Structures for III-V//Si Multi-Junction Solar Cells with Efficiency > 33%

Benedikt Bläsi*[1], Oliver Höhn[a], Hubert Hauser[a], Nico Tucher[a,b], Romain Cariou[a], Jan Benick[a], Frank Feldmann[a,b], Paul Beutel[a], David Lackner[a], Gerald Siefer[a], Stefan W. Glunz[a,b], Andreas W. Bett[a], Frank Dimroth[a] and Martin Hermle[a]

[a] Fraunhofer Institute for Solar Energy Systems ISE, Heidenhofstraße 2, 79100 Freiburg, Germany;
[b] Albert-Ludwigs-University, Department of Sustainable Systems Engineering INATECH, Georges-Köhler-Allee 103, 79110 Freiburg, Germany;

ABSTRACT

Silicon based multi-junction solar cells are a promising option to overcome the theoretical efficiency limit of a silicon solar cell (29.4%). With III-V semiconductors, high bandgap materials applicable for top cells are available. For the application of such silicon based multi-junction devices, a full integration of all solar cell layers in one 2-terminal device is of great advantage. We realized a triple-junction device by wafer-bonding two III-V-based top cells onto the silicon bottom cell. However, in such a series connected solar cell system, the currents of all sub-cells need to be matched in order to achieve highest efficiencies. To fulfil the current matching condition and maximise the power output, photonic structures were investigated. The reference system without photonic structures, a triple-junction cell with identical GaInP/GaAs top cells, suffered from a current limitation by the weakly absorbing indirect semiconductor silicon bottom cell. Therefore rear side diffraction gratings manufactured by nanoimprint lithography were implemented to trap the infrared light and boost the solar cell current by more than 1 mA/cm^2. Since planar passivated surfaces with an additional photonic structure (i.e. electrically planar but optically structured) were used, the optical gain could be realized without deterioration of the electrical cell properties, leading to a strong efficiency increase of 1.9% absolute. With this technology, an efficiency of 33.3% could be achieved.

Keywords: Multi-junction solar cells, III-V solar cells, Silicon solar cells, diffraction gratings, optical modelling, nanoimprint lithography, light trapping, photon management

1. INTRODUCTION

The efficiency of single-junction solar cells is limited due to the poor energetic utilization of the solar spectrum. A substantial part of the incident power cannot be used due to thermalization losses for short wavelength radiation and transmission or escape losses for long wavelength radiation (Fig. 1 left). The Shockley-Queisser radiative efficiency limit [1] of a single junction solar cell under AM 1.5G spectral irradiance according to ASTM G173-03 with an optimal band gap of 1.34 eV is 33% [2]. For silicon, which is the dominating absorber material in PV, the intrinsic Auger recombination limits the efficiency to 29.4% [3]. Additional loss mechanisms in realistic devices further reduce the practical efficiency limit to approximately 27% [4]. Given that the current record efficiency is 26.7% [5] there is not much more room for improvement for single-junction silicon solar cells.

* Email: benedikt.blaesi@ise.fraunhofer.de, Tel: +49 (0) 761 4588 5995, Fax: +49 (0) 761 4588-9995

Photonics for Solar Energy Systems VII, edited by Ralf B. Wehrspohn, Alexander N. Sprafke, Proc. of SPIE Vol. 10688, 1068803 · © 2018 SPIE · CCC code: 0277-786X/18/$18 · doi: 10.1117/12.2307831

A promising way to overcome these limits is the use of silicon-based multi-junction solar cells. This approach allows the reduction of thermalization and transmission losses (Fig. 1 right), resulting in Shockley-Queisser radiative efficiency limits of 41.9% for a two-junction device (top cell bandgap 1.73 eV) and 46.1% for a triple-junction cell (top and middle cell bandgaps 2.01 eV/1.50 eV) [6]. The individual subcells can be interconnected in different ways: (i) the multi-terminal approach with mechanical stacking and separate electrical contacting of each subcell or (ii) the series interconnection of the subcells resulting in a two terminal device. While the multi-terminal approach offers potentially slightly higher efficiencies [7], the final module integration is much more challenging. Due to the simple drop in solution for module manufacturing, two-terminal devices are of great interest from an application point of view. Due to the series interconnection, the subcell with the lowest current limits the overall current of the multi-junction cell.

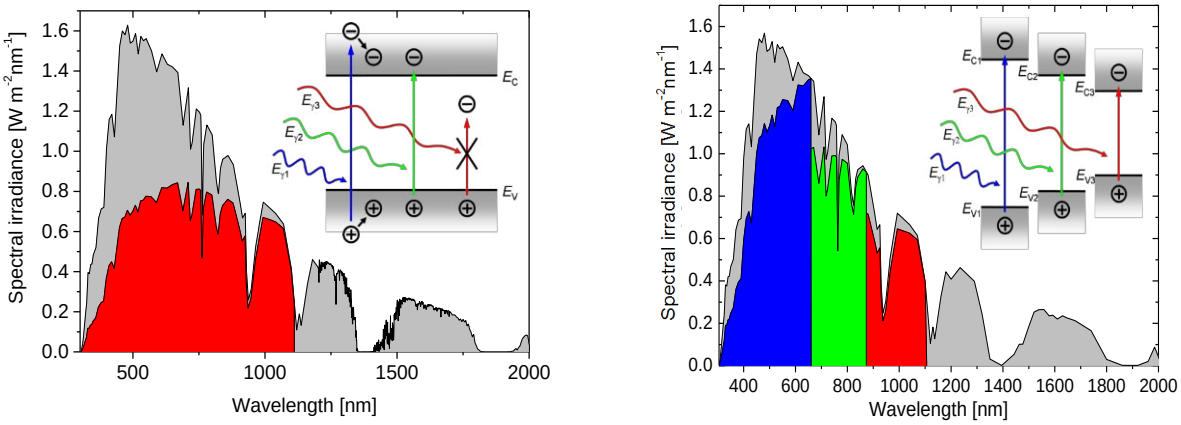

Figure 1: Usable fractions of the solar spectrum AM1.5g for a single junction silicon solar cell (left) and a silicon based triple junction solar cell (right).

For the silicon based multi-junction cells, two top cell material classes attract the most attention. While perovskites are a very promising candidate for low cost processes, III-V semiconductors have shown their potential for highest efficiencies and stability e.g. in concentrating applications [5]. However, the direct epitaxial growth of a III-V multi-junction solar cell on to silicon is very challenging due to the lattice mismatch between silicon an GaAs [8]. With surface-activated wafer bonding as known from microelectronics technology, this problem could be circumvented [9]. However, the silicon surface has to be flat to be compatible with the wafer bonding process. Thus the standard approach for a good light trapping, upright pyramids, cannot be used. Therefore an alternative light trapping structure, which is essential for an indirect semiconductor like silicon, has to be placed at the rear side of the cell.

In this paper, at first the solar cell concept is described (section 2) and then the rear side light trapping concept is introduced (section 3). Afterwards, the solar cell results are presented (section 4) and analysed with the aid of OPTOS simulations (Optical Properties of Textured Optical Sheets, section 5).

2. THE CELL CONCEPT

A planar silicon bottom cell featuring poly-Si/SiO_x passivating contacts [10,11] on both sides has been used. This layer stack leads to a very good surface passivation and does not suffer from the wafer bonding process. With these contacts, a very high open circuit voltage can be achieved. As top and middle cell materials for the triple-junction device $Ga_{0.51}In_{0.49}P$ and GaAs were chosen. The III-V cells were epitaxially grown on a GaAs wafer and bonded to the silicon bottom cell. Then the GaAs wafer was removed by an etching process [9] and a double layer antireflection coating (DARC, 65 nm Ta_2O_5 +110 nm MgF_2) was deposited. Finally, a front metal grid as well as a silver rear contact was applied. The result is a monolithic triple-junction two-terminal device with successfully implemented passivating contacts (Fig. 2, [12]).

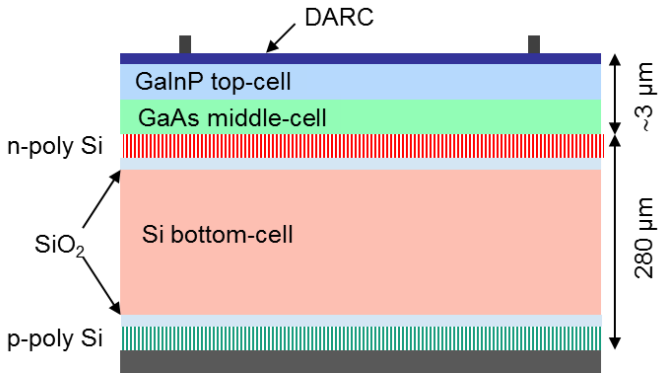

Figure 2: Basic monolithic triple cell architecture, consisting of III-V top and middle cells and a silicon bottom cell with passivating contacts.

The device described so far features only planar interfaces and will be called "planar cell" in the remainder of this article. On one 4-inch wafer, 12 cells with area 4 cm^2 and 4 cells with area 1 cm^2 were processed. The best cell was characterized at Fraunhofer ISE CalLab, with the results shown in Table 1 and in Figure 3 [12].

Table 1: Solar cell parameters of the planar cell, as measured by Fraunhofer ISE CalLab [12].

V_{oc} [V]	J_{sc} [mA/cm^2]	*FF* [%]	η [%]
3.125	11.6	86.5	31.4

These results show that very high open circuit voltage (V_{oc}) and fill factor (FF) values could be achieved. Electroluminescence measurements showed that the voltages of the subcells are 1.412 V (top cell), 1.024 V (middle cell) and 0.692 V (bottom cell) [12]. These values prove the excellent passivation quality. The excellent FF shows the low contact resistance. However, the cell suffers from a relatively low short circuit current (I_{sc}). The reason for this can be seen from the external quantum efficiencies (EQE, Figure 3). The EQE of the bottom cell drops for wavelengths > 1000 nm, indicating a low IR absorption. This is no surprise, since in the planar device there is no light trapping. The consequence is a significantly lower current for the bottom cell (11.6 mA/cm^2) compared to top cell (13.1 mA/cm^2) and middle cell (12.7 mA/cm^2). This means that the silicon bottom cell limits the current of the triple-junction cell.

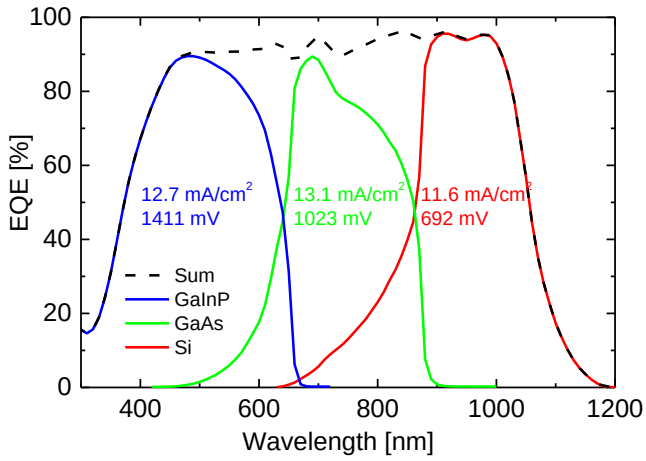

Figure 3: EQE of the planar cell [12]. The poor light harvesting for wavelengths > 1000 nm and the resulting current mismatch can clearly be seen.

3. INTEGRATION OF REAR SIDE LIGHT TRAPPING STRUCTURE

One way to achieve current matching could be an adjustment of the top and middle cell band gaps. But this would not solve the problem of the poor light harvesting in the infrared. In order to improve the light harvesting, light trapping structures can be employed. Since pyramidal textures at the GaAs-Si interface are not compatible with wafer bonding technology, photonic rear side structures were implemented.

For such photonic rear side structures, three key requirements must be fulfilled:

(1) The near infrared absorption in the silicon must be enhanced,
(2) the high passivation quality must be maintained and
(3) a very good electrical contact must be ensured [13].

For requirement (1), diffraction gratings are very well suited. Such gratings have first been proposed by Kiess and Morf [14]. More recent design studies as well as experimental results showed that crossed or hexagonal gratings with a period around 1 µm are very well suited for single junction crystalline silicon solar cells as well as for silicon bottom cells in tandem devices [13,15–18]. For requirement (2), it is very beneficial to keep the interface relevant for surface recombination planar while at the same time introducing the optical structure (EPOS concept: electrically planar, optically structured [19]). The rear surface with passivating contacts as implemented in the planar cell described above is an excellent starting point for the implementation of an EPOS rear side. So we took the planar cell and removed rear metallization. Following this step, the rear side photonic structure was implemented as follows [12]:

At first, a binary crossed grating with a period of 1 µm and a depth of 250 nm was originated by interference lithography [20,21]. From this master structure, a copy was made by electroplating, followed by the fabrication of a cast molded polydimethylsiloxane (PDMS) stamp. This stamp was used in the subsequent nanoimprint lithography (NIL) step. After spin coating of SU-8 photoresist [22] to the rear surface of the cell, the grating was transferred in a thermally assisted roller-ultraviolet-NIL process [23–25]. In order to allow for a good electrical rear side contact (requirement 3), resist residuals between the pillars were removed by reactive ion etching (RIE) using oxygen/argon plasma. In addition to the resist removal, this process step introduced a nano roughness on top of the resist pillars. As final steps, HF dip and silver evaporation were performed, ensuring a good ohmic rear contact. For an overview of the process steps see Fig. 4.

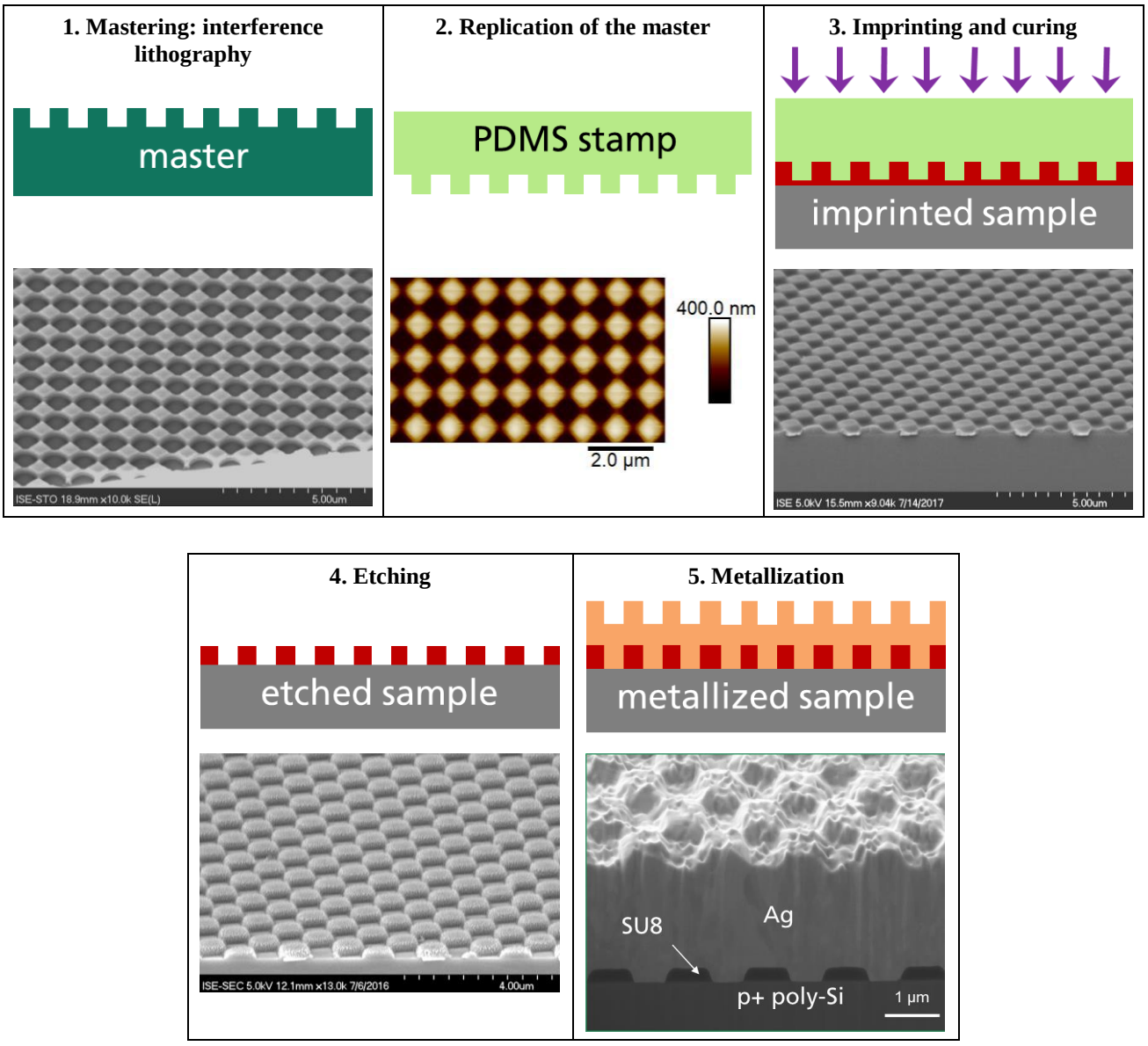

Figure 4: Schematic view of the process chain for the fabrication of the photonic rear side.

The resulting solar cell with rear side diffraction grating, in the following called “grating cell”, is schematically shown in Fig. 5. This procedure enabled us to investigate the identical solar cell stack, just with a different rear side [12]. So the direct comparison is possible, and all differences can be attributed to the changes in the rear side.

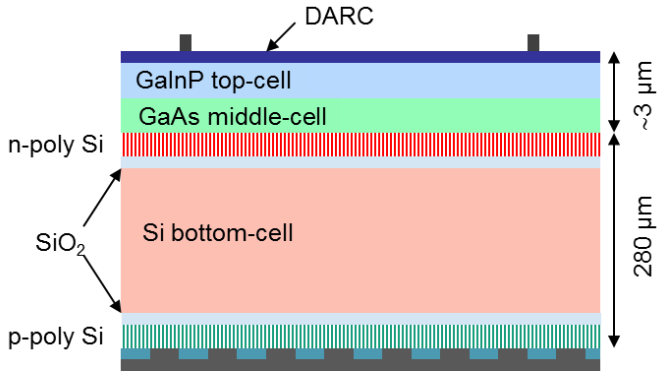

Figure 5: Basic structure of the solar cell with a rear side diffraction grating ("grating cell").

4. SOLAR CELL RESULTS: PLANAR VERSUS GRATING

The EQE comparison (Fig. 5) of planar versus grating cell shows that both cells perform identically up to approximately 1000 nm. Since all radiation with wavelengths < 1000 nm is absorbed before it can reach the rear side, this highlights that, apart from the rear surface, the cell stack was not modified by the grating process. In the spectral range between 1000 nm and 1200 nm, however, the EQE is enhanced for the grating cell. The enhancement amounts to a current increase of 1.1 mA/cm^2. This proves that the light trapping could be implemented successfully and condition (1) could be fulfilled.

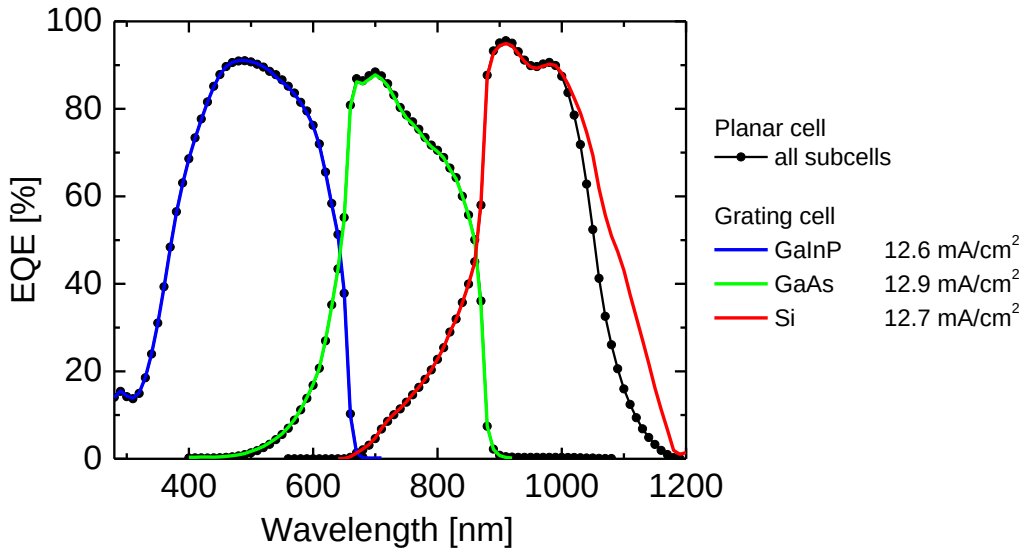

Figure 6: EQEs of planar and grating cell. Note the grating induced enhancement for wavelengths > 1000 nm.

It is very instructive to have a closer look at the optical performance in the IR spectral region. Looking at the reflectance measurements (Fig. 6), one can see a strong reduction introduced by the rear side grating. In fact, the reduction amounts to 2.1 mA/cm^2, which is substantially more than the EQE increase. Consequently, there is a relevant fraction of the absorbed photons which cannot be converted to electricity. This parasitic absorptance (calculated as 1 – EQE – R) is plotted in Fig. 7. There is a moderate parasitic absorptance for wavelengths > 1000 nm in the planar cell, which can be attributed to the rear side. For the grating cell, the parasitic absorptance is strongly increased, which hints towards a substantial loss mechanism connected to the rear side reflection.

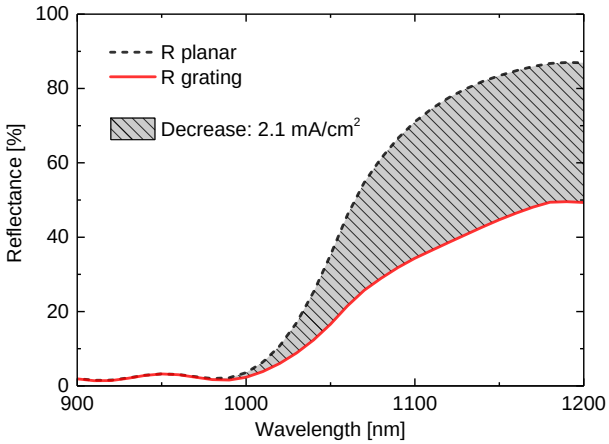

Figure 7: Reflectance curves of planar and grating cell

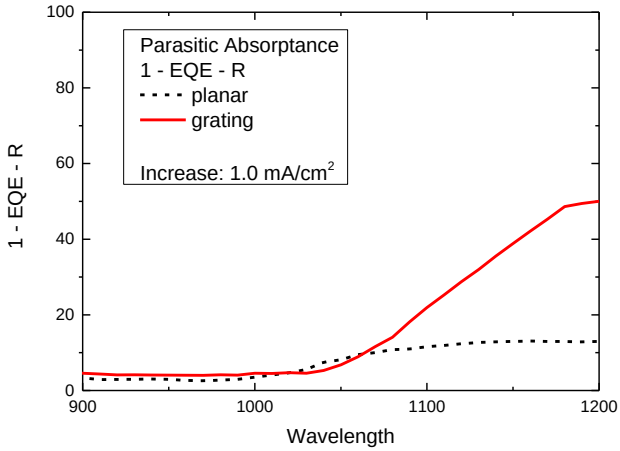

Figure 8: Parasitic absorption in planar and grating cell

Of course, improving the EQE is not sufficient in order to improve the overall solar cell performance. The solar cell parameters of planar and grating cell are shown in Table 2. It is apparent that the EQE enhancement directly translates into a J_{sc} increase by the same amount (1.1 mA/cm^2). The V_{oc} values show that the photonic rear side could be implemented without degrading the excellent rear surface passivation. So, condition 2 could also be fulfilled. For the FF, the grating cell shows a slightly lower value. This was to be expected since for multi-junction cells in two-terminal configuration the FF is lower if the currents of the subcells are matched [26]. Nevertheless, the overall conversion efficiency could be boosted by 1.9% absolute, reaching a new record efficiency of 33.3% [12].

Table 2: Solar cell parameters of planar and grating cell, as measured by Fraunhofer ISE CalLab [12].

	V_{oc} [V]	J_{sc} [mA/cm^2]	*FF* [%]	η [%]
Planar cell	3.125	11.6	86.5	31.4
Grating cell	3.127	12.7	83.8	33.3

5. INTERPRETATION AND COMPARISON WITH OPTOS MODELING

Optical modeling can play a crucial role for understanding the measured solar cell results as well as for optimizing future devices. However, tandem solar cells featuring small scale structures like diffractive gratings cannot be modeled with standard methods like ray tracing. The OPTOS formalism [17,27] has already been demonstrated to be highly suitably for simulating solar cells with a diffractive grating at the rear side [18]. An extension of the OPTOS enabling the separate absorptance calculation for all considered material layers is required for modeling tandem solar cell and will be published elsewhere [28]. For the III-V-on-silicon solar cell investigated in this work, this extension allows for an investigation of the current matching between the different subcells as well as parasitic absorption losses.

Figure 9 shows a comparison of OPTOS absorptance simulation results and EQE measurements of the planar and grating cells. The OPTOS simulation of the planar cell (black - dotted) fits well to the measured EQE data (black – solid). The front side metallization of the experimental device is taken into account in the simulation by reducing the light incidence by 1.5%. Looking at the grating cell, it is the structured metal grating which is difficult to model due to the required high computational resources. As approximation, redistribution matrices of a silicon grating with 1 µm period, surrounding air and a planar metal rear reflector (see right side of Figure 9) were calculated and used in an OPTOS simulation. The result (blue - dotted curve) shows a very high absorption in the near infrared spectral region, which is due to strongly enhanced light trapping properties by the diffractive grating. The corresponding current gain compared to the planar cell would be as high as 2.8 mA/cm^2. However, this simulation result describing an idealized grating does not agree well with the

experimental result of the structured metal grating. This is not surprising as a structured metal interface is likely to increase the parasitic absorption [29]. To account for this effect, 25% parasitic absorption were added artificially to the rear side reflection redistribution matrices of the silicon grating, reducing the reflectance at every rear side interaction. For more details of this simulation approach and its application to silicon single junction solar cells see reference [18]. As can be seen from the red dotted curve in Figure 9, this approach leads to a very good agreement between simulation and experiment for the silicon bottom cell.

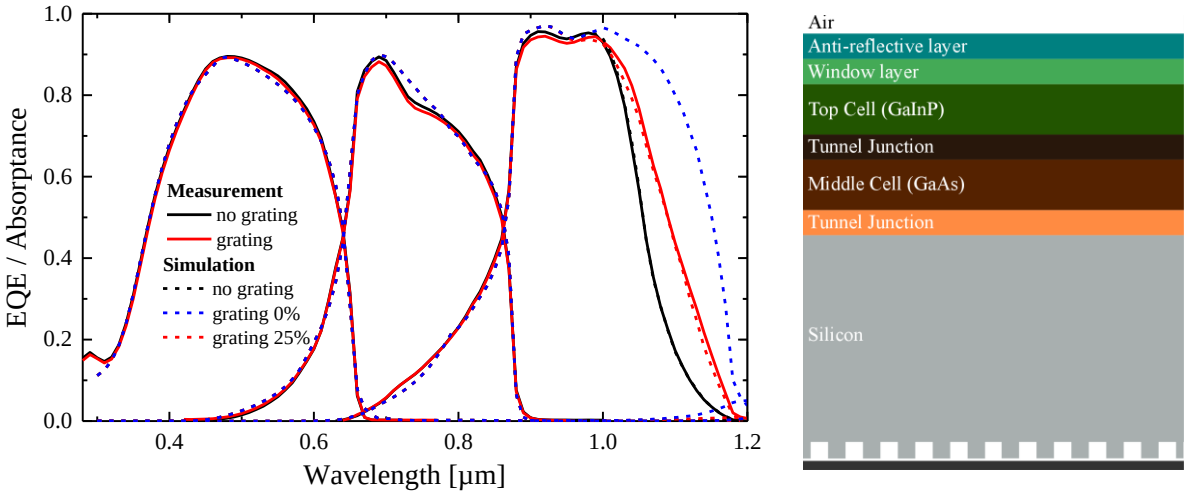

Figure 9: Left: Measured EQE and simulated absorptance of the planar and grating cell. Simulating the idealized diffractive grating (0% absorption at each interaction) underestimates the parasitic absorption due to the structured metal reflector in the experimental device. Introducing additional 25% parasitic absorption as simplified representation of the metal grating loss leads to a good agreement with the EQE measurement results. Right: Sketch of the modeled solar cell.

OPTOS allows for an even more detailed analysis by taking into account reflection losses as well as parasitic absorption in further layers, such as the anti-reflective coating, the window-layer, tunnel junctions and the rear side metal. This kind of loss analysis was carried out for the grating cell assuming 25% additional parasitic absorption at the rear side, which performs similarly as the record device. The results are depicted in Figure 10 including the corresponding reflected or absorbed photocurrent density values that were calculated by weighting with the AM1.5g spectrum and integration.

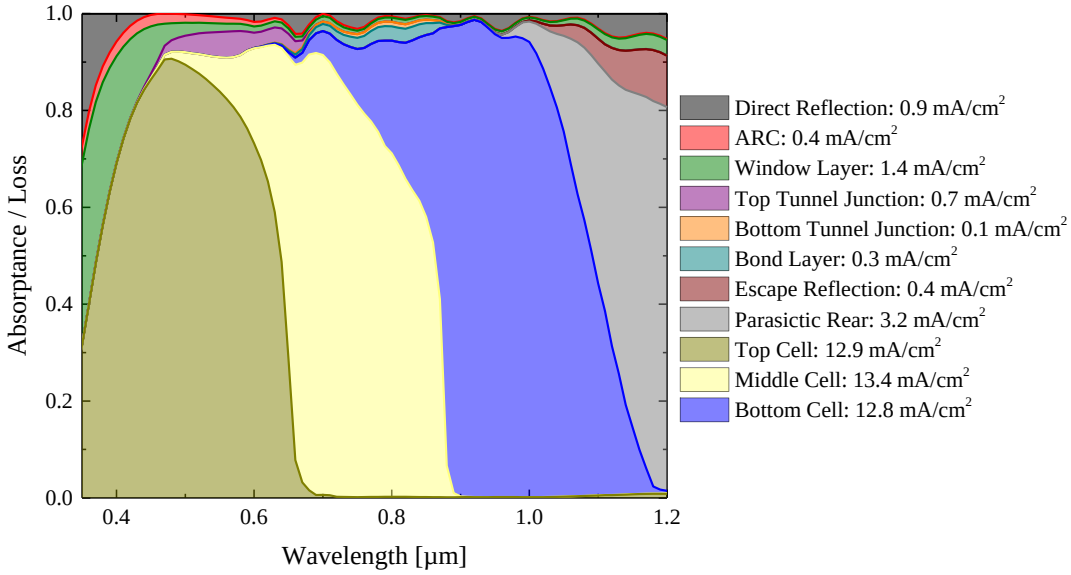

Figure 10: Optical loss analysis of the solar cell configuration with dielectric rear side grating and 25% additional parasitic absorption, including the corresponding photocurrent density values. Front side metallization is not taken into account here.

Most of the material layers of this III-V-on-silicon tandem solar cell show parasitic absorption, at least for a small wavelength range. For example, the window layer and the top tunnel junction reduce the available photocurrent density by 1.4 mA/cm^2 and 0.7 mA/cm^2, respectively. All parasitic losses increase for wavelengths > 1000 nm since the light trapping structure causes multiple interactions. The parasitic rear side absorption even reaches a value of 80% at 1200 nm and accounts for 3.2 mA/cm^2. If we keep the measured values of the parasitic absorptance (Fig. 8) in mind (50% at 1200 nm), it becomes clear, that the model strongly overestimates the parasitic rear side absorption. Nevertheless, the grating cell suffers from high parasitic absorption. This loss mechanism must be addressed in further optimization steps. A realistic estimation of the potential photocurrent density gain due to improvements of the grating fabrication can be based on the modeling result without parasitic absorption shown in Figure 9. The resulting bottom cell photocurrent density in that case is, with a value of 14.5 mA/cm^2, significantly higher than the measured 12.7 mA/cm^2 (grating cell) and the 11.6 mA/cm^2 (planar cell).

6. CONCLUSION AND OUTLOOK

With the integration of a rear side light trapping structure, the current of the silicon bottom cell within a two-terminal III-V-on-silicon triple-junction solar cell could be boosted. At the same time, passivation quality and ohmic rear side contact could be maintained at the same excellent level as for the planar reference cell. With this, a new record conversion efficiency of 33.3% could be achieved. Modeling based on the OPTOS formalism enables the detailed analysis of the light trapping effects and loss mechanisms. The analysis of the grating solar cell showed that parasitic absorption at the rear side leads to major losses.

As a consequence of these findings, several improvements are planned as further developments:

In order to better understand the loss mechanisms and to optimize the photonic structure design, a full wave optical description of the metal structure as input for OPTOS is needed. Possible ways to go are a reduction of the nano roughness of the metal or an improvement of the light redirection of the rear side structure. To achieve the latter goal, non-periodic, quasi-random or tailored disorder structures are a promising option. Such structures have already been investigated by several groups [30–32]. A very promising approach for the origination of such structures is interference lithography (Fig. 11), as has already been shown in earlier publications [21]. For the subsequent process chain, the technologies described in this work can be applied. Another interesting fabrication technology could be the phase separation of incompatible polymers as was shown by Walheim et al [33], and has recently been proposed for solar cell applications [34].

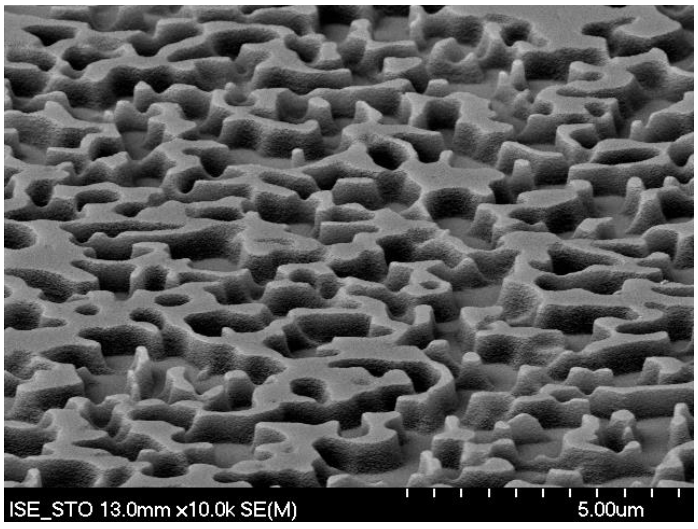

Figure 11: Non-periodic photoresist structure originated by interference lithography. The defined spatial frequency spectrum makes such structures very promising candidates for rear side light trapping [21].

ACKNOWLEDGEMENTS

This project has received funding from:

- *European Union's Horizon 2020 research and innovation programm* under grant agreement No 727497 (**SiTaSol**) and No 641023 (**NanoTandem**)
- Marie Sklodowska-Curie grant N°655272
- German Federal Ministry for Economic Affairs and Energy under contract number 0324247 (**PoTaSi**)

The authors would like to thank S. Seitz, A. Seiler, A. Leimenstoll, F. Schätzle, A. Lösel, R. Freitas, V. Klinger, E. Oliva, E. Schäffer, A. Wekkeli, E. Fehrenbacher, V. Kübler and M. Schachtner for their support with interference lithography, cell processing and measurements.

The authors would like to thank C. Flötgen, N. Razek and M. Wimplinger from EVG for wafer bonding.

REFERENCES

[1] W. Shockley and H. J. Queisser, "Detailed Balance Limit of Efficiency of p-n Junction Solar Cells," J. Appl. Phys. **32**, 510 (1961).
[2] S. Rühle, "Tabulated values of the Shockley–Queisser limit for single junction solar cells," Solar Energy **130**, 139–147 (2016).
[3] A. Richter, M. Hermle, and S. W. Glunz, "Reassessment of the limiting efficiency for crystalline silicon solar cells," IEEE Journal of Photovoltaics **3**, 1184–1191 (2013).
[4] D. D. Smith, P. Cousins, S. Westerberg, R. de Jesus-Tabajonda, G. Aniero, and S. Yu-Chen, "Toward the Practical Limits of Silicon Solar Cells," Photovoltaics, IEEE Journal of **4**, 1465–1469 (2014).
[5] M. A. Green, Y. Hishikawa, E. D. Dunlop, D. H. Levi, J. Hohl-Ebinger, and A. W.Y. Ho-Baillie, "Solar cell efficiency tables (version 51)," Prog Photovolt Res Appl **26**, 3–12 (2018).
[6] K.-H. Lee, K. Araki, L. Wang, N. Kojima, Y. Ohshita, and M. Yamaguchi, "Assessing material qualities and efficiency limits of III-V on silicon solar cells using external radiative efficiency," Prog. Photovolt: Res. Appl. **24**, 1310–1318 (2016).
[7] S. Essig, C. Allebé, T. Remo, J. F. Geisz, M. A. Steiner, K. Horowitz, L. Barraud, J. S. Ward, M. Schnabel, A. Descoeudres, D. L. Young, M. Woodhouse, M. Despeisse, C. Ballif, and A. Tamboli, "Raising the one-sun conversion efficiency of III–V/Si solar cells to 32.8% for two junctions and 35.9% for three junctions," Nat. Energy **2**, 17144 (2017).
[8] T. J. Grassman, M. R. Brenner, S. Rajagopalan, R. Unocic, R. Dehoff, M. Mills, H. Fraser, and S. A. Ringel, "Control and elimination of nucleation-related defects in GaP/Si(001) heteroepitaxy," Appl. Phys. Lett. **94**, 232106 (2009).
[9] R. Cariou, J. Benick, P. Beutel, N. Razek, C. Flotgen, M. Hermle, D. Lackner, S. W. Glunz, A. W. Bett, M. Wimplinger, and F. Dimroth, "Monolithic Two-Terminal III–V//Si Triple-Junction Solar Cells With 30.2% Efficiency Under 1-Sun AM1.5g," IEEE J. Photovoltaics **7**, 367–373 (2017).
[10] F. Feldmann, M. Bivour, C. Reichel, M. Hermle, and S. W. Glunz, "Passivated rear contacts for high-efficiency n-type Si solar cells providing high interface passivation quality and excellent transport characteristics," Solar Energy Materials & Solar Cells **120, Part A**, 270–274 (2014).
[11] F. Feldmann, C. Reichel, and M. Hermle, "The application of poly-Si/SiO x contacts as passivated top/rear contacts in Si solar cells," Solar Energy Materials and Solar Cells **159**, 265–271 (2017).
[12] R. Cariou, J. Benick, F. Feldmann, O. Höhn, H. Hauser, P. Beutel, N. Razek, M. Wimplinger, B. Bläsi, D. Lackner, M. Hermle, G. Siefer, S. W. Glunz, A. W. Bett, and F. Dimroth, "III–V-on-silicon solar cells reaching 33% photoconversion efficiency in two-terminal configuration," Nat. Energy **17**, 183 (2018).
[13] J. Eisenlohr, B. G. Lee, J. Benick, F. Feldmann, M. Drießen, N. Milenkovic, B. Bläsi, J. C. Goldschmidt, and M. Hermle, "Rear side sphere gratings for improved light trapping in crystalline silicon single junction and silicon-based tandem solar cells," Solar Energy Materials & Solar Cells **142**, 60–65 (2015).

[14] H. Kiess and R. Morf, "Light Trapping In Solar Cells And Determination Of The Absorbed Energy By Calorimetry," in *Optical Materials Technology for Energy Efficiency and Solar Energy Conversion VIII*, Vol. 1149 of Proceedings of SPIE (1989), p. 124.
[15] A. Mellor, I. Tobias, A. Marti, M. J. Mendes, and A. Luque, "Upper limits to absorption enhancement in thick solar cells using diffraction gratings," Prog Photovoltaics **19**, 676–687 (2011).
[16] M. Peters, M. Rüdiger, H. Hauser, M. Hermle, and B. Bläsi, "Diffractive gratings for crystalline silicon solar cells-optimum parameters and loss mechanisms," Prog. Photovolt: Res. Appl. **20**, 862–873 (2012).
[17] N. Tucher, J. Eisenlohr, P. Kiefel, O. Höhn, H. Hauser, M. Peters, C. Müller, J. C. Goldschmidt, and B. Bläsi, "3D optical simulation formalism OPTOS for textured silicon solar cells," Opt. Express **23**, A1720 (2015).
[18] J. Eisenlohr, N. Tucher, H. Hauser, M. Graf, J. Benick, B. Bläsi, J. C. Goldschmidt, and M. Hermle, "Efficiency increase of crystalline silicon solar cells with nanoimprinted rear side gratings for enhanced light trapping," Solar Energy Materials & Solar Cells **155**, 288–293 (2016).
[19] B. Bläsi, N. Tucher, J. Eisenlohr, B. G. Lee, J. Benick, H. Hauser, M. Hermle, and J. C. Goldschmidt, "Rear side gratings for silicon solar cells: efficiency enhancement finally demonstrated," in *Proc. of SPIE*, Proceedings of SPIE (SPIE, 2016), p. 98980.
[20] A. J. Wolf, H. Hauser, V. Kübler, C. Walk, O. Höhn, and B. Bläsi, "Origination of nano- and microstructures on large areas by interference lithography," Microelectron Eng **98**, 293–296 (2012).
[21] B. Bläsi, H. Hauser, C. Walk, B. Michl, A. Guttowski, A. Mellor, J. Benick, M. Peters, S. Jüchter, C. Wellens, V. Kübler, M. Hermle, and A. J. Wolf, "Photon management structures for solar cells," in *Proc. of SPIE*, Proceedings of SPIE (SPIE, 2012), 84380Q-84380Q-12.
[22] J. M. Shaw, J. D. Gelorme, N. C. LaBianca, W. E. Conley, and S. J. Holmes, "Negative photoresists for optical lithography," IBM J. Res. & Dev. **41**, 81–94 (1997).
[23] H. Hauser, B. Michl, S. Schwarzkopf, V. Kübler, C. Müller, M. Hermle, and B. Bläsi, "Honeycomb texturing of Silicon via nanoimprint lithography for solar cell applications," IEEE Journal of Photovoltaics **2**, 114–122 (2012).
[24] N. Tucher, O. Höhn, H. Hauser, C. Müller, and B. Bläsi, "Characterizing the degradation of PDMS stamps in nanoimprint lithography," Microelectronic Engineering **180**, 40–44 (2017).
[25] H. Hauser, N. Tucher, K. Tokai, P. Schneider, C. Wellens, A. Volk, S. Seitz, J. Benick, S. Barke, F. Dimroth, C. Müller, T. Glinsner, and B. Bläsi, "Development of nanoimprint processes for photovoltaic applications," J. Micro/Nanolith. MEMS MOEMS **14**, 31210 (2015).
[26] W. E. McMahon, K. E. Emery, D. J. Friedman, L. Ottoson, M. S. Young, J. S. Ward, C. M. Kramer, A. Duda, and S. Kurtz, "Fill factor as a probe of current-matching for GaInP 2 /GaAs tandem cells in a concentrator system during outdoor operation," Prog Photovolt Res Appl **16**, 213–224 (2008).
[27] J. Eisenlohr, N. Tucher, O. Höhn, H. Hauser, M. Peters, P. Kiefel, J. C. Goldschmidt, and B. Bläsi, "Matrix formalism for light propagation and absorption in thick textured optical sheets," Opt. Express **23**, A502 (2015).
[28] N. Tucher, O. Höhn, J. C. Goldschmidt, and B. Bläsi, "Optical modeling of structured silicon-based tandem solar cells and module stacks," submitted to Optics Express (2018).
[29] A. Mellor, H. Hauser, C. Wellens, J. Benick, J. Eisenlohr, M. Peters, A. Guttowski, I. Tobías, A. Martí, A. Luque, and B. Bläsi, "Nanoimprinted diffraction gratings for crystalline silicon solar cells. implementation, characterization and simulation," Opt. Express **21**, A295–A304 (2013).
[30] E. R. Martins, J. Li, Y. Liu, V. Depauw, Z. Chen, J. Zhou, and T. F. Krauss, "Deterministic quasi-random nanostructures for photon control," Nat Comms **4**, 2665 (2013).
[31] M.-C. van Lare and A. Polman, "Optimized Scattering Power Spectral Density of Photovoltaic Light-Trapping Patterns," ACS Photonics **2**, 822–831 (2015).
[32] P. M. Piechulla, L. Muehlenbein, R. B. Wehrspohn, S. Nanz, A. Abass, C. Rockstuhl, and A. Sprafke, "Fabrication of Nearly-Hyperuniform Substrates by Tailored Disorder for Photonic Applications," Advanced Optical Materials **18**, 1701272 (2018).
[33] S. Walheim, M. Böltau, J. Mlynek, G. Krausch, and U. Steiner, "Structure Formation via Polymer Demixing in Spin-Cast Films," Macromolecules **30**, 4995–5003 (1997).
[34] R. H. Siddique, Y. J. Donie, G. Gomard, S. Yalamanchili, T. Merdzhanova, U. Lemmer, and H. Hölscher, "Bioinspired phase-separated disordered nanostructures for thin photovoltaic absorbers," Sci. Adv. **3**, e1700232 (2017).